NASA TECHNICAL MEMORANDUM

NASA TM X-52457

NASA TM X-52457

RADIATION PROPERTIES OF A CdS SOLAR CELL AND VARIOUS METALS AT SPACE CONDITIONS

by John R. Jack and Ernie W. Spisz
Lewis Research Center
Cleveland, Ohio

TECHNICAL PAPER proposed for presentation at Third Space Simulation Conference sponsored by the Institute of Environmental Sciences, the American Institute of Aeronautics and Astronautics, and the American Society for Testing and Materials
Seattle, Washington, September 16-18, 1968

NATIONAL AERONAUTICS AND SPACE ADMINISTRATION · WASHINGTON, D.C. · 1968

RADIATION PROPERTIES OF A CdS SOLAR CELL AND VARIOUS METALS AT SPACE CONDITIONS

by John R. Jack and Ernie W. Spisz

Lewis Research Center
Cleveland, Ohio

TECHNICAL PAPER proposed for presentation at

Third Space Simulation Conference
sponsored by the Institute of Environmental Sciences,
the American Institute of Aeronautics and Astronautics,
and the American Society for Testing and Materials
Seattle, Washington, September 16-18, 1968

NATIONAL AERONAUTICS AND SPACE ADMINISTRATION

RADIATION PROPERTIES OF A CdS SOLAR CELL AND VARIOUS METALS AT SPACE CONDITIONS

by John R. Jack and Ernie W. Spisz
Lewis Research Center
National Aeronautics and Space Administration
Cleveland, Ohio

AUTHORS' AUTOBIOGRAPHIES

Mr. Jack, who is Head of the Environmental Physics Section, received his B.S. degree in physics and mathematics from Kent State University in 1946 and his M.S. degree from the Carnegie Institute of Technology in 1948. Mr. Jack joined the NASA Lewis research staff in July 1948 and since that time has conducted research on aerodynamic loads, boundary layer transition and heat transfer and electrothermal propulsion. Since 1965, he has specialized in research on environmental physics. He has written numerous NACA-NASA reports on these subjects and has been granted several patents associated with his work. He is a member of the AIAA.

Mr. Spisz is a research engineer in the Environmental Physics Section. He graduated from the University of Toledo with a BSME degree in 1955 after which he joined the General Electric Company. While at GE until 1962 he completed their three year Advanced Engineering Program and worked in the areas of heat transfer and aerodynamics on advanced jet engine concepts and on the development of electrothermal thrustors for space propulsion. Mr. Spisz joined the Lewis Research Center in 1962. While at Lewis he has been involved in electrothermal propulsion devices and in the measurement of radiation properties of materials. Mr. Spisz is a registered professional engineer and a member of AIAA.

INTRODUCTION

A great deal of interest in the thermal radiation properties of solids has been generated in the last few years by the rapid growth of our space program. For example, the normal solar absorptance and total hemispherical emittance of materials suitable for spacecraft are of particular importance because these parameters govern the thermal balance of the spacecraft and consequently the equilibrium temperature of the vehicle. In addition, since solar cell power supplies have been used successfully and probably will be used extensively for years to come, their optical properties and associated operating temperatures are desired so that a cell's electrical behavior can be predicted for a variety of environmental conditions. Because of the lack of theoretical methods to predict solar absorptance and hemispherical emittance over a wide temperature range, it is necessary, especially for composites, to rely upon experimental methods to meet the needs of present-day space technology. This paper describes the NASA Lewis program (which employs a new technique for measuring these properties) and presents the experimental results obtained for various metals as well as a CdS solar cell at temperatures ranging from 155° K to 520° K.

SYMBOLS

A amplitude of temperature perturbation during cyclic period, °K

c_p specific heat, joules/(gm)(°K)

I_o radiant intensity, joules/(cm^2)(sec)

I_1 radiant intensity at one astronomical unit, joules/cm^2 sec

i_o intensity amplitude at mean temperature during cyclic equilibrium, joules/(cm^2)(sec)

k intensity perturbation factor

m test sample mass per unit area, gms/cm^2

q all heat exchange terms other than those specified by the remaining terms in equation one, joules/(cm^2)(sec)

r distance from sun, AU

T test sample temperature, °K

$\dot{T}$ time rate of temperature change, °K/sec

T_m mean cyclic temperature of sample, °K

t time, seconds

α solar absorptance of front surface

ϵ_b hemispherical emittance of back surface of sample

ϵ_f hemispherical emittance of front surface of sample

θ' time constant of material, seconds

σ Stefan-Boltzmann constant, joules/(cm^2)(sec)(°K^4)

φ phase angle between sample temperature and cyclic incident radiation, radians

ω cyclic frequency, rad/sec

THEORETICAL BACKGROUND

The method used herein to determine optical properties is described in detail in reference 1. The physical model consists of a thin sample suspended in an ultra high vacuum, cold-wall environment. A radiant intensity, I_o, is imposed normal to one surface of the sample to establish its equilibrium temperature, T_m. The intensity is then perturbed sinusoidally with amplitude kI_o (where $k < 1.0$) and frequency ω.

The differential equation describing the temperature of an isothermal sample is, from reference 1

$$mc_p\dot{T} = \alpha I_o(1 + k \sin \omega t) + q - (\epsilon_f + \epsilon_b)\sigma T^4 \qquad (1)$$

where ϵ_f and ϵ_b are the front and back surface emittance, respectively and q contains all heat exchange terms other than those specified by the remaining terms in equation 1.

Within the very small temperature range resulting from the intensity perturbation, the material properties (c_p, α, and ϵ) and the heat exchange term q are considered independent of temperature. In addition, under these conditions the T^4 term can be linearized about T_m as $T^4 = 4T_m^3T - 3T_m^4$. With these assumptions, the solution of equation (1) is given by

$$T = T_m + A\left[\sin(\omega t - \varphi) + e^{-t/\theta'}\sin\varphi\right] \qquad (2)$$

The phase angle, φ, and temperature amplitude, A, are related to the test sample properties by

$$\varphi = \tan^{-1}\omega\theta' \qquad (3)$$

and

$$A = \left(\frac{\alpha I_o k}{mc_p}\right)\left[\left(\frac{1}{\theta'}\right)^2 + \omega^2\right]^{-1/2} \qquad (4)$$

where θ', the time constant of the material, is given by

$$\theta' = \frac{mc_p}{4(\epsilon_f + \epsilon_b)\sigma T_m^3} = \frac{1}{\omega}\tan\varphi \qquad (5)$$

At cyclic equilibrium (i.e., when $e^{-t/\theta'}\sin\varphi$ becomes negligible) the temperature response is sinusoidal around T_m with amplitude, A, and phase angle, φ. Therefore, by measuring the phase angle φ, the frequency ω, the temperature amplitude A and the intensity perturbation amplitude kI_o, both emittance and solar absorptance can be determined from equations (4) and (5) provided the specific heat variation with temperature is known for the test sample.

APPARATUS AND PROCEDURE

Environmental Facility

The application of the theory described in the previous section requires a high vacuum, cold-wall facility to eliminate residual gas conduction and to achieve low sample temperatures. Figure 1 is a schematic drawing of the high vacuum facility and the experimental arrangement used. The facility is the Solar Space Environment Simulator Facility developed in 1960 at the Lewis Research Center and modified in 1966. The original oil diffusion and mechanical pumps have been replaced by liquid nitrogen cryosorption pumps to eliminate oil backstreaming and possible contamination of the test surfaces. The facility is initially pumped to 10^{-4} torr by the liquid nitrogen cryosorption pumps. The annular wall of the test section and baffles are then filled with liquid helium to cryopump the chamber below 10^{-10} torr and also provide a 4 °K radiation background. The four liquid helium cooled baffles within the test section reduce stray radiation and permit the imposed collimated radiation to reach the model.

Samples and Mount

The metal samples are 1 cm wide by 2 cm long and are approximately 0.00254 cm (0.001 in.) thick. The samples are suspended in the test plane by four 0.00254 cm (0.001 in.) wires which are spot welded at each of the four corners of the sample. Two of the four wires are a matched-pair Chromel-constantan thermocouple and the other two wires are either Chromel or constantan. In all cases small diameter wires are used for the sample supports and thermocouple to minimize their effect on the thermal response of the sample.

The pure metal samples are high purity (99.99%+) and the surfaces were used in the "as received" condition. All metal samples were cleaned in alcohol, the thermocouple and support wires welded in place and the sample cleaned again in alcohol. After the final cleaning, the samples were not handled and the exposure to atmospheric conditions was limited to the period required to install the samples in the environmental simulator.

The solar cell used in this investigation is a current state-of-the-art thin-film cadmium sulfide cell having a total area of 54.75 cm^2. The laminated composition and fabrication of a typical thin film CdS solar cell of this type is discussed in detail in reference 2. Mounting of the solar cell was accomplished by suspending it in the environmental facility from four 26-gage copper wires fastened to the solar cell by an epoxy adhesive. The cell temperature was measured with a 36-gage copper-constant thermocouple epoxied to the rear-center of the cell.

Solar Simulator

The solar simulator consists of a 12 kw carbon arc with associated collimating optics (fig. 1). The simulator output is a collimated beam with a maximum intensity of 250 mW/cm^2. Intensity can be continuously varied by the moveable zoom lens up to plus or minus ten percent of a given setting. Low intensity levels are obtained with the 12 KW arc by using apertures and/or fine wire mesh screens that act as neutral density filters (ref. 3). In addition a 1 KW, quartz-iodine tungsten filament lamp can be substituted for the 12 KW arc to provide stable, low intensity radiation suitable for material time constant and emittance determinations.

Sinusoidal intensity perturbations are provided by automatic control of the movable zoom lens. The control system is composed of a calibrated silicon solar cell which is coupled with a reference sine generator into a differential amplifier that actuates a balancing motor to maintain the proper position of the zoom lens. The reference sine signal can be varied to produce both the desired amplitude and the cyclic frequency of the sinusoidal perturbation.

Solar Simulator Spectral Distribution

The spectral energy distribution of the solar simulator was measured with a Perkin-Elmer Model 99 spectrometer that had been calibrated by a transfer method over a wavelength range of 0.25 to 2.5 μ. That is, the spectrometer entrance slit was illuminated by a spectrally calibrated 1000-watt, quartz-iodine tungsten filament lamp whose calibration was traceable to an NBS standard of spectral irradiance. The spectral distribution of the 12 KW carbon arc solar simulator, obtained experimentally, is compared in figure 2 with the Johnson curve (ref. 4). This comparison is based upon making the radiant energy available from the carbon arc spectrum equal to that available from the Johnson spectrum over the wavelength interval 0.35 μ to 2.5 μ. Agreement of the carbon arc curve with the Johnson curve is good

over the wavelength region of interest, 0.35 μ to 2.0 μ.

Measurements and Accuracy

Data were recorded on a multi-channel strip chart recorder and an X-Y recorder. The strip chart recorder monitors the radiant intensity and solar cell thermocouple to insure the constancy of the absolute intensity level and cyclic frequency. The X-Y recorder is the primary data recording instrument. At cyclic equilibrium, a typical X-Y recorder trace over one cycle provides an elliptical Lissajous figure such as that shown in figure 3. The reference sinusoidal intensity signal (or the calibrated solar cell signal) is recorded on the x-axis and the test sample temperature on the y-axis. The actual data trace is large with sufficient resolution to insure accurate measurements of the mean sample temperature T_m, the amplitude of the temperature oscillation A, the initial intensity level I_o, the amplitude of the intensity perturbation kI_o, and the intensity amplitude at the mean sample temperature i_o. From geometrical consideration of figure 3 (ref. 5), the phase angle between the sample temperature and radiant intensity at cyclic equilibrium is given by

$$\varphi = \tan^{-1}\left[\left(\frac{kI_o}{i_o}\right)^2 - 1\right]^{-1/2} \qquad (6)$$

The emittance as determined from equation (5) is

$$(\epsilon_f + \epsilon_b) = \frac{\omega m c_p}{4T_m^3 \tan\varphi}$$

The relative error in the emittance determination (e.g., ref. 6), neglecting errors in the cyclic frequency and material heat capacity, is

$$\frac{\delta(\epsilon_f + \epsilon_b)}{\epsilon_f + \epsilon_b} = 3\frac{\delta T_m}{T_m} + \frac{\delta(\tan\varphi)}{\tan\varphi} \qquad (7)$$

For temperatures greater than 250° K the temperature measurement errors are small and the predominating error is due to the inaccuracies in the measurement of the phase angle (or rather $\tan\varphi$). The relative error in the measurement of $\tan\varphi$ (eq. (6)) is

$$\frac{\delta(\tan\varphi)}{\tan\varphi} = (1 + \tan^2\varphi)\left[\frac{\delta(kI_o)}{kI_o} + \frac{\delta(i_o)}{i_o}\right] \qquad (8)$$

For values of $\tan\varphi > 1.0$ the error increases rapidly with increasing values of the phase angle. Generally the phase angle is limited to less than seventy degrees in order to obtain accurate emittance data. However, the phase angle must be maintained greater than forty degrees otherwise the Lissajous figures become slender and the intensity amplitude measurement errors become predominant.

The absorptance as determined from equation (4) is

$$\alpha = \frac{\omega A m c_p}{kI_o}\left(\frac{1}{\tan^2\varphi} + 1\right)^{1/2}$$

In addition to the phase angle measurement, the temperature amplitude measurement is required. The relative error in absorptance is given by

$$\frac{\delta(\alpha)}{\alpha} = \frac{\delta(A)}{A} + \frac{\delta(kI_o)}{kI_o} + \left(\frac{1}{\tan^2\varphi + 1}\right)\frac{\delta(\tan\varphi)}{\tan\varphi} \qquad (9)$$

The critical considerations are primarily the errors involved in the temperature and intensity amplitude measurements. The error due to $\tan\varphi$ measurements is not as important for absorptance determinations as it is in emittance determinations. In fact, the larger the value of $\tan\varphi$, the less effect it has on the absorptance.

Accuracy of the experimental data for optical properties was estimated from the uncertainties arising from the individual basic measurements. The relative error of the absorptance-emittance ratio was determined from these uncertainties and calculated to be approximately ±5 percent.

RESULTS AND DISCUSSION

Metal Optical Properties

The optical properties (ϵ, α, α/ϵ) of 304 stainless steel, aluminum, platinum, nickel and molybdenum were obtained. These data are shown in figure 4 for temperatures ranging from approximately 230° K to 520° K. It should be noted that, for the metals, the front and back surface emittances are considered equal (see eqs. (1) and (5)). In general, the hemispherical emittance of each metal increases with increasing temperature, the solar absorptance is approximately constant and the absorptance-emittance ratio decreases with increasing temperature. The absorptance-emittance ratio decrease with temperature is thus primarily due to the emittance increase.

Our research effort to determine the optical properties of metals is a continuing effort. After determining the optical properties of various satelite materials and coatings at temperatures varying from 150° K to 500° K, our model support system will be modified to include a cooling-heating system so that data at temperatures less than 150° K and greater than 500° K can be obtained.

Solar Cell Optical Properties

The optical properties of the CdS cell were obtained at temperatures corresponding to radiant intensities that varied from 0.028 to 1.02 solar constants. The time constants (eq. (5)) as determined from the measured phase angles and imposed frequencies are shown in figure 5 as a function of cell temperature. The time constant increases with decreasing temperature (eq. (5)) and the longest time constant obtained is 143 seconds at a cell temperature of 156° K. Two data points obtained with the 1-KW tungsten filament bulb as the radiation source are also included in figure 5 since the cell time constant is unaffected by the source spectral distribution. Data from the 1-KW bulb should be more accurate than that obtained with the arc lamp because of the absolute stability of the 1 KW lamp. Nevertheless all the time constants are consistent regardless of the source used. Data from either the carbon arc or the 1 KW bulb can be used to obtain emittance. However, unlike the emittance determination, the 1 KW bulb data cannot be used in obtaining absorptance since its spectral distribution is not comparable to that of the sun.

The emittance and absorptance data evaluated from equations (4) and (5) are presented in figures 6 and 7 in terms of the heat capacity per unit area of the cell. Presentation in this form was necessary because specific heat data are not available for CdS solar cells. However, the plots can be utilized to obtain emittance and absorptance when specific heat data becomes available as a function of temperature. As a point of information, it should be noted that the measured cell temperatures are slightly higher than would occur when the cell was generating power. Calculations indicate that, for a cell having an electrical conversion efficiency of 5 percent, the cell temperature, while producing power, may be as much as 6° K lower than that presented herein.

The important optical parameter that establishes the cell's operating temperature is the absorptance-emittance ratio. This ratio can readily be obtained from the curves presented in figures 6 and 7. The absorptance-emittance ratio is shown in figure 8 for cell temperatures ranging from approximately 155° to 325° K. The important trend to note is the rapid decrease in the absorptance-emittance ratio as the temperature is increased. As the temperature increases from 155° to about 200° K, the absorptance-emittance ratio decreases from 0.70 to about 0.43, a decrease of 39 percent. This rapid decrease may be due to an increase in emittance from 155° K to 185° K. A further increase in temperature beyond 200° K produces little change; the α/ϵ ratio remains approximately constant at a value of 0.43 up to 325° K. Comparison of the 300° K experimental point presented in reference 7 with the preceding data shows good agreement.

For those interested in the mission aspects of the problem, the radiation intensity, cell equilibrium temperature, optical property data, and distance from the sun are all interrelated, in the ideal case, by the following equation

$$(\epsilon_f + \epsilon_b)\sigma T^4 = \frac{\alpha I_1}{r^2} \qquad (10)$$

where I_1 is the radiant intensity at 1 AU ($140\ mW/cm^2$) and r is the distance from the sun in astronomical units.

The experimental absorptance-emittance ratios are plotted as a function of distance from the sun (as obtained from eq. (10)) in figure 9. This plot indicates that the absorptance-emittance ratio is approximately constant from 0.90 to 3 AU or until an orbit approximately midway between Mars and Jupiter is reached. From there out into the solar system, the absorptance-emittance ratio apparently increases at a substantial rate.

SUMMARY OF RESULTS

Simulated space environmental tests were conducted on five prospective spacecraft metals and a current state-of-the-art thin film cadmium sulfide solar cell. Optical properties were investigated over a wide range of temperatures. The following results are considered important.

In general, over a temperature range of 230° K to 520° K, the hemispherical emittance of the metals increases with increasing temperature, the solar absorptance is approximately constant and the absorptance-emittance ratio decreases with increasing temperature.

The absorptance-emittance ratio of the CdS solar cell was found to be approximately constant with a value of 0.43 over the temperature range from 200° to 325° K. Below 200° K, the α/ϵ ratio increased rapidly to 0.70 at a temperature of 155° K. The cause of the rapid increase is believed to be the result of an emittance decrease with decreasing temperature.

REFERENCES

1. Jack, J. R., "Technique for Measuring Absorptance and Emittance by Using Cyclic Incident Radiation." AIAA Journal, Vol. 5 (1967), pp. 1603-1606.

2. Shirland, F. A. and F. Augustine, "Thin Film Plastic Substrate CdS Solar Cells." Vol. II, part C of the Proceedings of the Fifth Photovoltaic Specialists Conference (1965).

3. Heidt, L. J. and D. E. Bosley, "An Evaluation of Two Simple Methods for Calibrating Wavelength and Absorbtance Scales of Modern Spectrophotometers." Journal of the Optical Society of America, Vol. 43 (1953), pp. 760-766.

4. Johnson, F. S., "The Solar Constant." Journal of Meteorology, Vol. 11 (1954), pp. 431-439.

5. Terman, F. E. and J. M. Pettit, Electronic Measurements, 2nd ed., New York: McGraw-Hill Book Co., Inc. (1952).

6. Nelson, K. E. and J. T. Bevans, "Errors of the Calorimetric Method of Total Emittance Measurement." Measurement of Thermal Radiation Properties of Solids, NASA SP-31 (1963), pp. 55-65.

7. Liebert, C. H. and R. R. Hibbard, Theoretical Temperatures of Thin-Film Solar Cells in Earth Orbit. NASA TN D-4331 (1968).

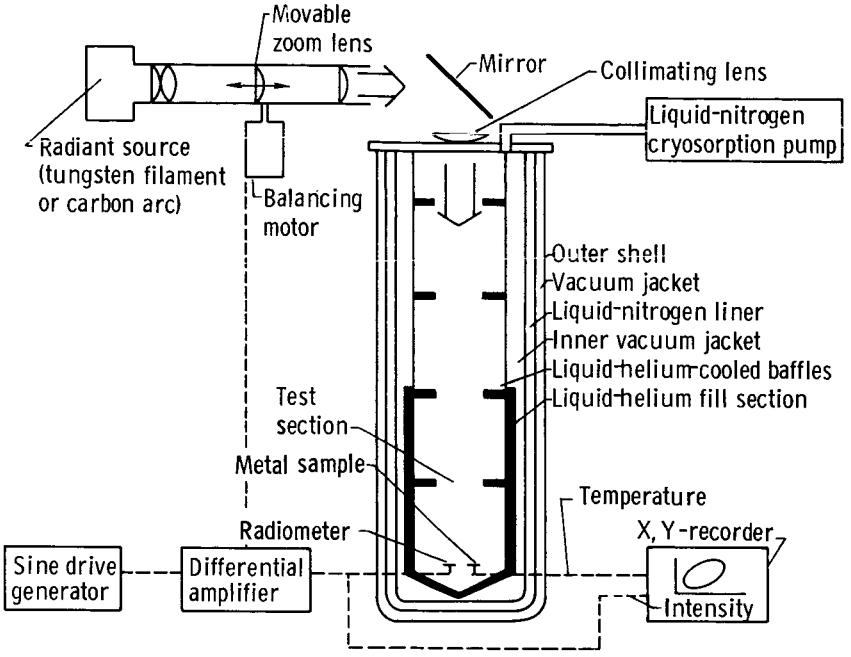

Figure 1. - Schematic drawing of experimental setup.

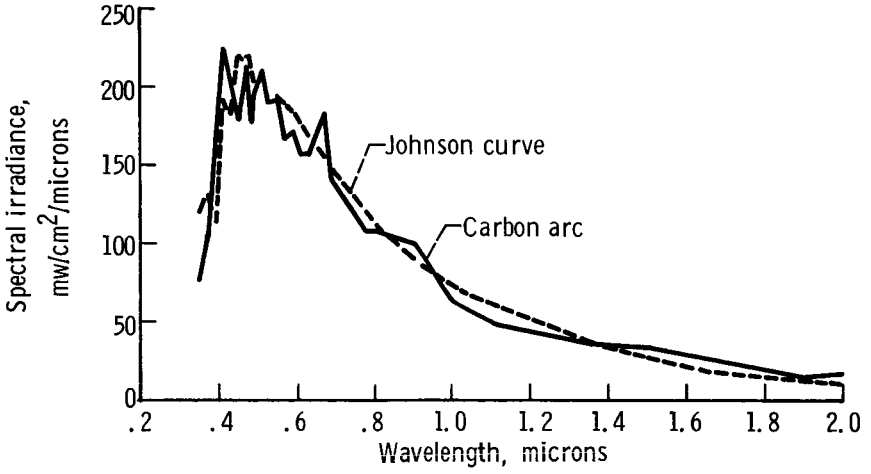

Figure 2. - Spectral irradiance of carbon arc solar simulator.

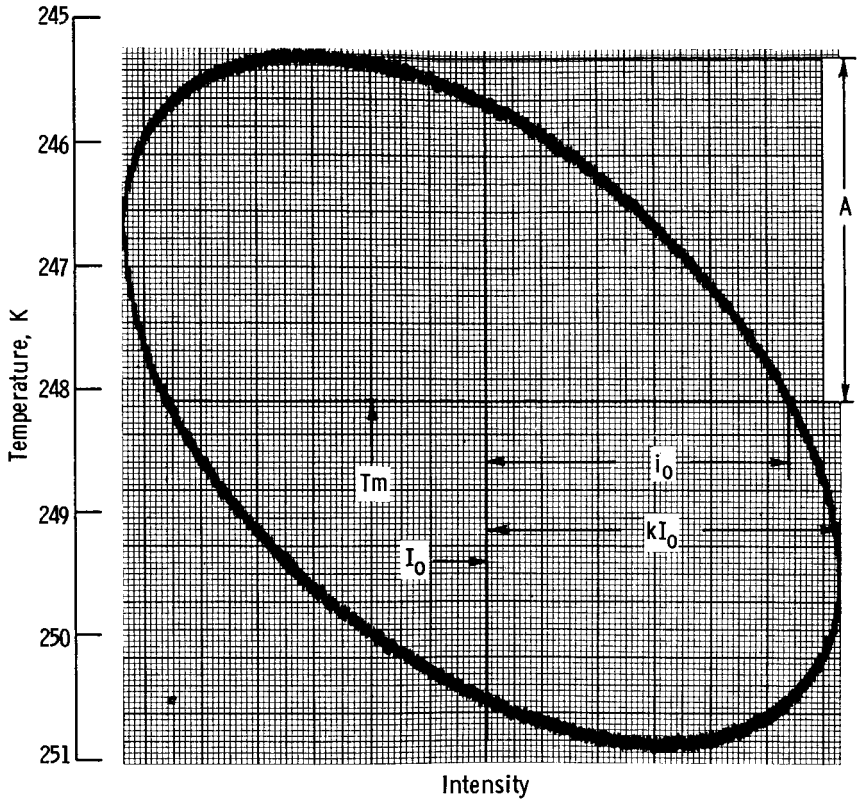

Figure 3. - X, Y-recorder figure for SS304 at 10 revolutions per hour.

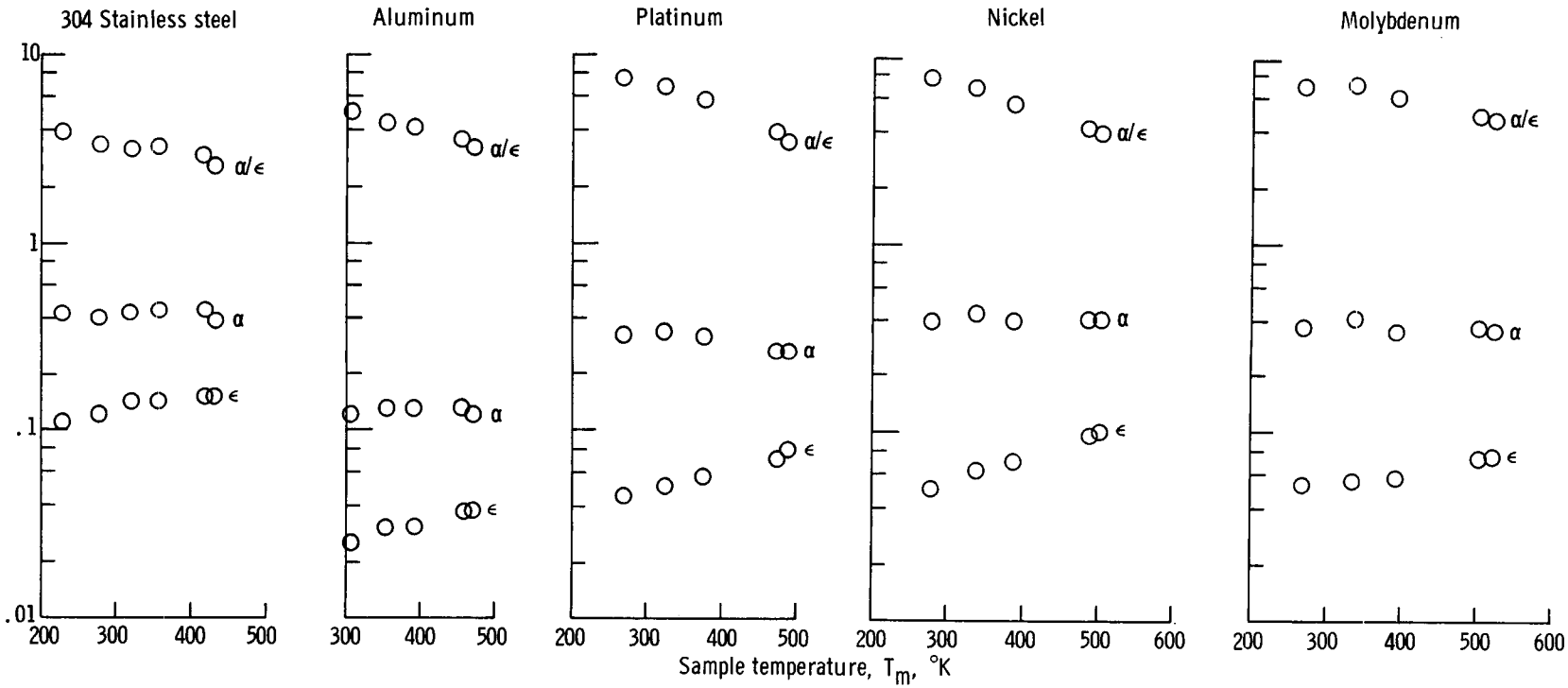

Figure 4. - Radiation properties of 304 stainless steel, aluminum, platinum, nickel and molybdenum.

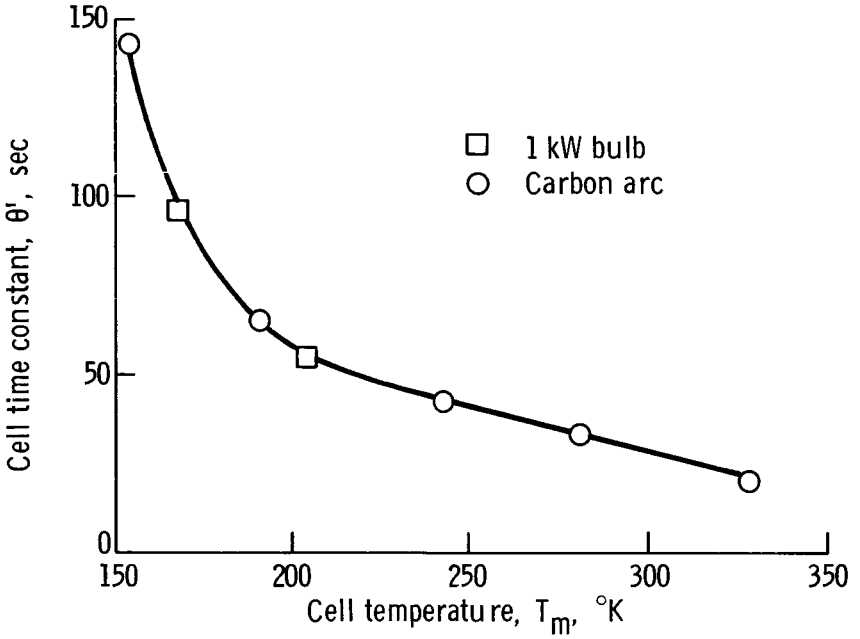

Figure 5. - Time constant of CdS solar cell.

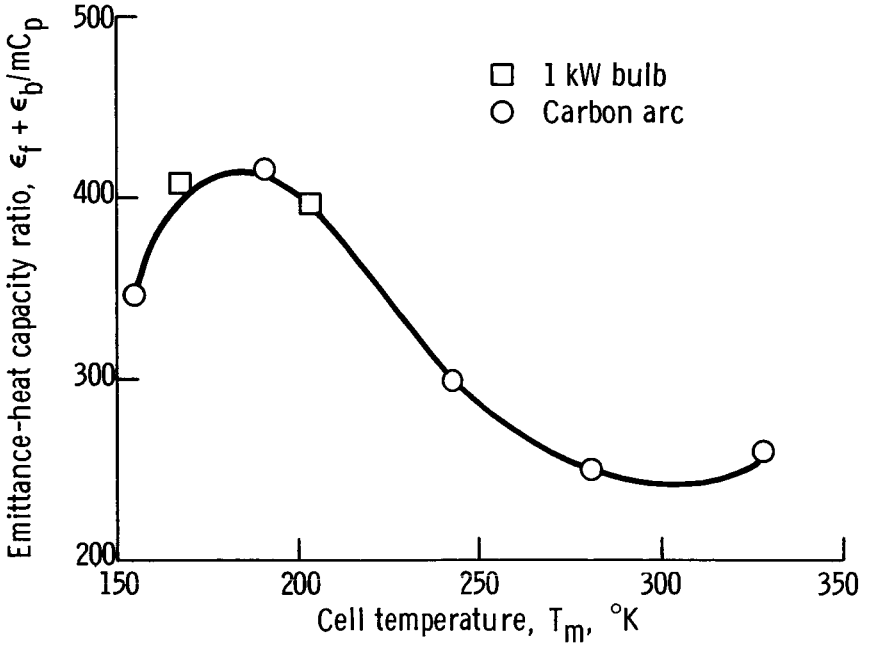

Figure 6. - Emittance of CdS solar cell.

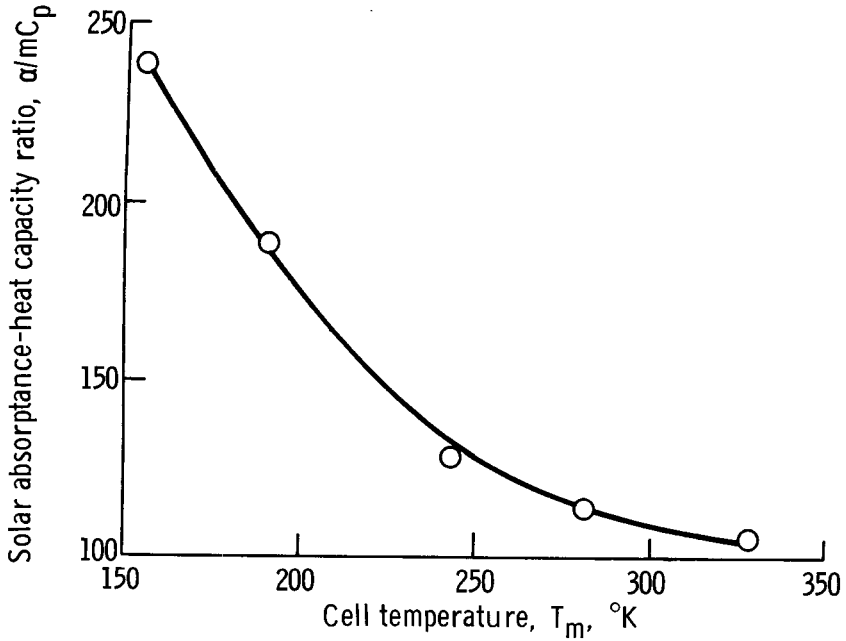

Figure 7. - Solar absorptance of CdS solar cell (carbon arc source).

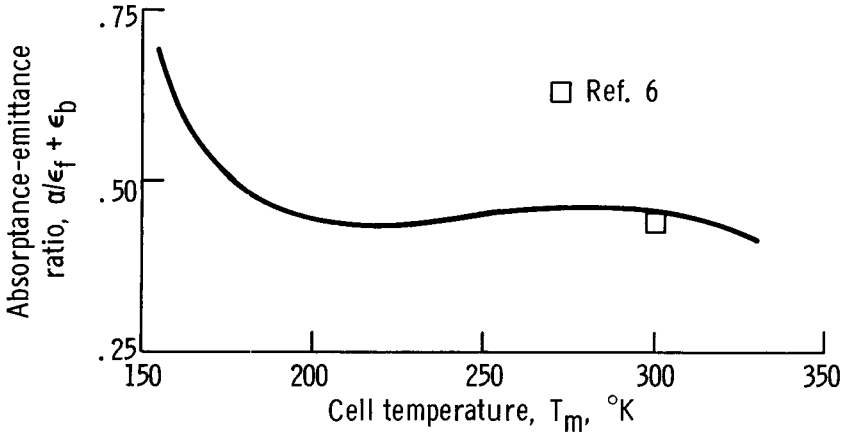

Figure 8. - Absorptance-emittance ratio for CdS solar cell.

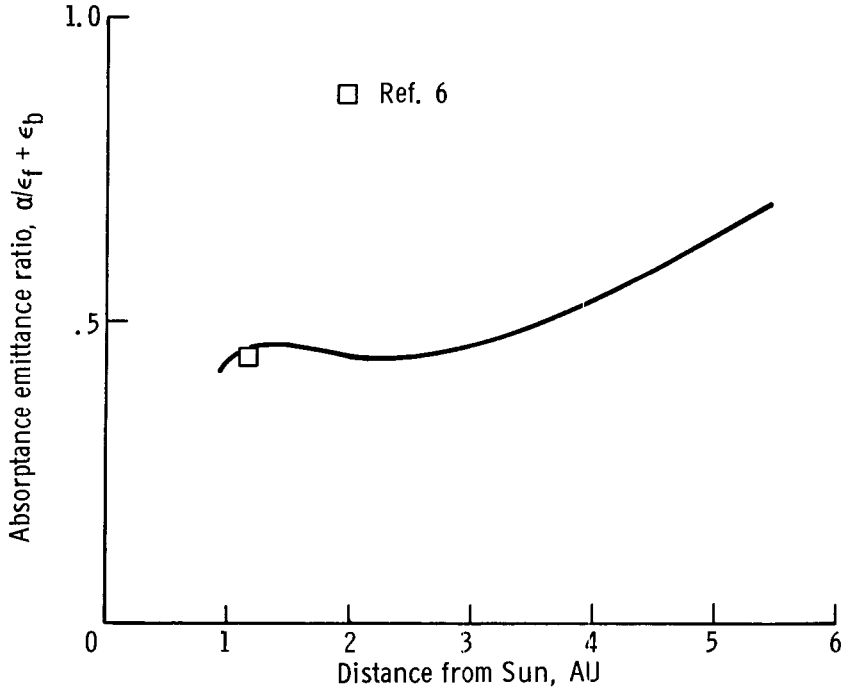

Figure 9. - Absorptance-emittance ratio of CdS solar cell at various distances from the Sun.

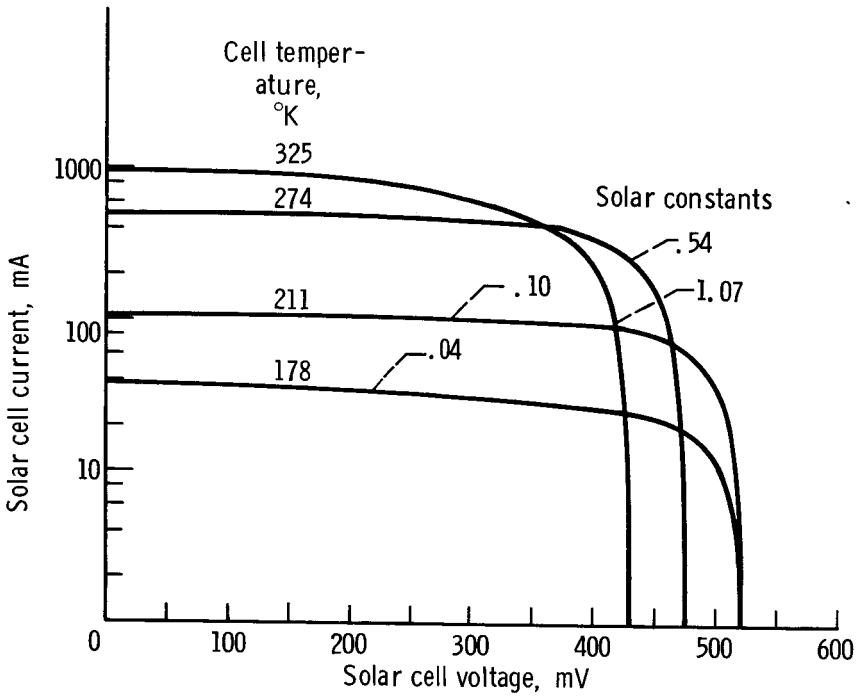

Figure 10. - Electrical characteristics of a CdS solar cell at various simulated solar radiation intensities.

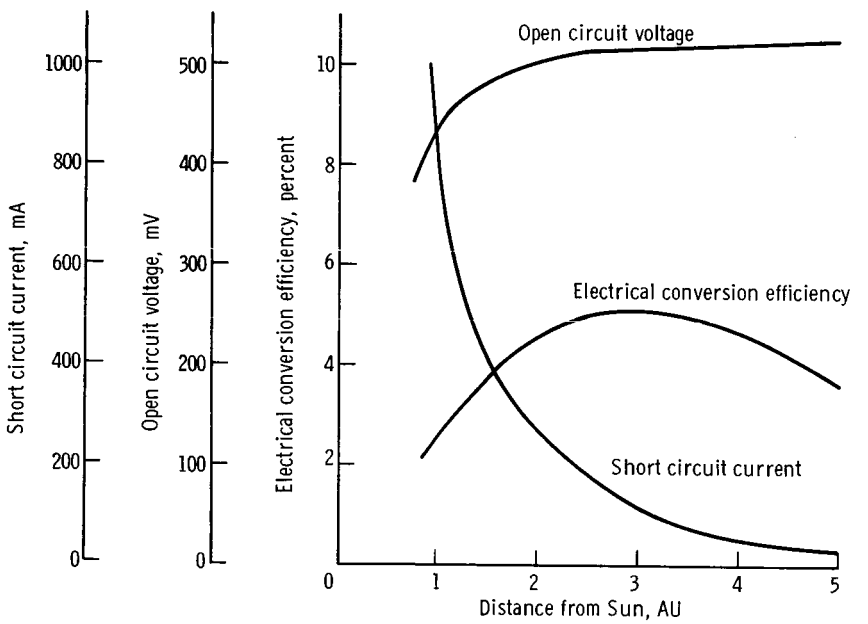

Figure 11. - Performance of CdS solar cell at various distances from the Sun.